Available online at www.sciencedirect.com
SCIENCE DIRECT®
Surface Science 565 (2004) 243–250
SURFACE SCIENCE
www.elsevier.com/locate/susc

Behavior of benzene on Zr(0001): effect of electron bombardment on benzene desorption profiles

N. Stojilovic, J.C. Tokash, R.D. Ramsier *

Departments of Physics, Chemistry, and Chemical Engineering, The University of Akron, 250 Buchtel Commons, Ayer Hall 111, Akron, OH 44325-4001, USA

Received 8 April 2004; accepted for publication 12 July 2004
Available online 29 July 2004

Abstract

We investigate the interaction of benzene (C_6H_6) with Zr(0001) and the effects of 500 eV electron bombardment. Two desorption states are resolved above 700 K in temperature programmed desorption (TPD) experiments. Electron bombardment has no significant effects on the amount of desorbing benzene but effects TPD profiles and desorption temperatures. We observe the production of C_2H_2 and C_4H_4 species for lower benzene exposures and detect no effect of electron bombardment on this trend. The C(KLL) Auger electron feature exhibits qualitative line-shape changes with respect to benzene exposure and annealing temperature. Our results indicate that benzene dissociates on Zr(0001) for lower exposures, forming a carbonized surface upon which additional benzene adsorbs and remains stable to unexpectedly high temperatures.

Keywords: Zirconium; Aromatics; Auger electron spectroscopy; Thermal desorption; Electron bombardment

1. Introduction

Zirconium, like titanium, is a getter material that is very reactive with respect to numerous molecules. As a consequence, cleaning the surface of this material from common impurities such as carbon is extremely difficult. Room temperature adsorption of various molecules on zirconium surfaces typically results in no or very little subsequent thermal desorption [1]. Dissolution of dissociated molecules into the bulk of the metal during heating occurs instead. It is of both fundamental and applied interest to investigate the interaction of carbon-containing molecules with gettering metal surfaces. In addition, electron-bombardment studies of zirconium might lead to a better understanding of surface reactions occurring in nuclear applications where zirconium

* Corresponding author. Tel.: +1 330 972 4936; fax: +1 330 972 6918.
E-mail address: rex@uakron.edu (R.D. Ramsier).

0039-6028/$ - see front matter © 2004 Elsevier B.V. All rights reserved.
doi:10.1016/j.susc.2004.07.015

alloys, as structural materials, are in the presence of radiolytic hyperthermal species.

The interest to study benzene as a model for more complicated aromatic molecules on metal surfaces is well known, and the interaction of benzene with well-defined single crystal surfaces has been investigated extensively [2–14]. The adsorption and thermal desorption behavior of C_6H_6 on Zr(0001) under ultra-high vacuum conditions has already been investigated in our laboratory [15,16]. By backfilling the vacuum system we found that following adsorption at 150 or 170 K only benzene and its cracking fragments desorbed near 715 K. This unusually high desorption temperature, together with an increase in oxygen Auger features induced by benzene adsorption, warrant further study. The C_6H_6/Zr(0001) system is now investigated using a capillary-array molecular beam doser for benzene exposure instead of backfilling. We now resolve two features in temperature programmed desorption (TPD) experiments and investigate the effects of electron bombardment on these features.

2. Experimental details

The stainless steel ultra-high vacuum chamber, together with the pumping system, has been described earlier [17,18]. Previously, exposure of Zr(0001) to various gases was accomplished by backfilling the chamber. Now a capillary-array molecular beam doser has been installed. Fig. 1 shows the molecular beam doser designed and built by the authors. It should be noted here that our chamber has a horizontal 4-axis sample manipulator, requiring the doser design to include a 90° bend.

The inlet and outlet gas line tube is 0.64 cm diameter 316 stainless steel with Cajon VCR-4 fittings. To limit the gas flow, a 2-μm diameter laser-drilled pinhole VCR seal is installed. The body of the doser is 304 stainless steel. A glass capillary array (Burle Electro-Optics) with a pore diameter of 10 μm and zero bias angle is press-fit to the exit of the doser with an end cap that is constructed out of the same 304 stainless steel. Careful attention was given to the mating surfaces between the doser body, glass capillary array, and the end cap. The metal surfaces were ground flat to better seal the doser assembly and prevent leaks around the array. After the end cap was pressed onto the doser body, it was spot welded in place. All butt welds in the construction are vacuum compatible. The entire construction is mounted to a linear motion mechanism (Kurt J. Lesker UHV LSM 38-50 conflat with double bellows) with 5.1 cm of travel so that the doser can be retracted while other experiments are taking place.

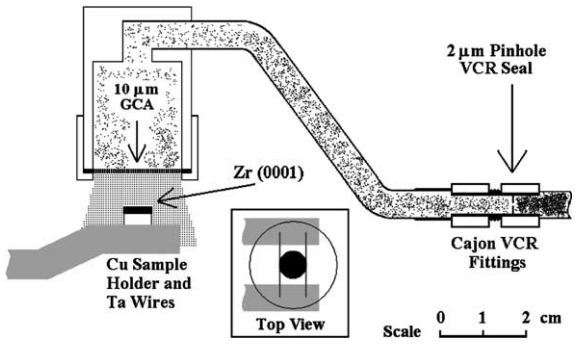

Fig. 1. Cross-sectional schematic of the molecular beam doser. The sample holder shown rotates about an axis that lies along a left-to-right direction across the figure. The inset shows what the sample holder assembly looks like rotated 90° toward the viewer. The circle shown in the inset indicates the area of the glass capillary-array doser.

The total particle flux out of the doser was calculated using the effusion equation. Calibration data was also recorded on the rate of change of pressure in the gas line versus time during dosing. After correcting for geometric flux-interception factors, the exposure directly to the sample surface is expressed in molecules/cm^2. Using the molecular beam doser only a small part of the sample holder, in addition to the Zr(0001) surface, is exposed to reactive gas, thus significantly reducing the possibility of artifacts in TPD experiments.

The radius and thickness of the cylindrically shaped zirconium single crystal are 3 and 1 mm, respectively. The crystal is polished on one side to 30 nm and the uncertainty in orientation of the (0001) plane is below 1°. The crystal is heated resistively through tantalum wires that are spot-welded to the sample. The sample is cooled from one side using a copper braid attached to a liq-

uid-nitrogen cold finger and temperatures slightly below 150 K can be achieved.

Cleaning of the surface is performed by several cycles of Ar^+ (2 keV, 2 $\mu A\,cm^{-2}$) bombardment followed by annealing to approximately 860 K. Sputtering is performed at approximately 160 K. The cleanliness of the surface is monitored by Auger electron spectroscopy (AES). We point out here that some carbon and oxygen are left on the surface prior to experiments since reducing their amounts below detection limits requires prolonged annealing and sputtering at higher temperatures, which on the other hand induces sulfur segregation to the surface. Zr(MNV) and S(LMM) features overlap which makes determination of sulfur content very difficult. We have previously investigated the interaction of SO_2 with Zr(0001) [19] and demonstrated that near-surface sulfur can be minimized by our cleaning procedure. It is more important in the present work to suppress the S rather than the residual C and O, which is a trade-off that must be made in working with this reactive metal system.

Experiments were conducted at a base pressure of $\sim 1 \times 10^{-10}$ Torr. Benzene (Fisher, purity > 99.0 %) was further purified via several freeze-pump-thaw cycles. Prior to every C_6H_6 dose the gas-handling manifold was pumped by a turbo-molecular pump. The heating rate in TPD and step-wise annealing AES experiments was 1.8 K/s. Auger spectra were taken at approximately 150 K with 3 keV beam energy and 15 $\mu A\,cm^{-2}$ current density. The sample was positioned in line-of-sight with respect to a quadrupole mass spectrometer (QMS) during TPD experiments. The increase in background pressure during dosing benzene was a factor of ~10, as measured by an ion gage.

3. Results and discussion

3.1. Temperature programmed desorption

Fig. 2 presents TPD spectra of benzene following adsorption of benzene at 150 K. The spectra elucidate how the TPD profiles change as a function of exposure. The same adsorption temperature (150 K) and the same heating rate (1.8 K/s)

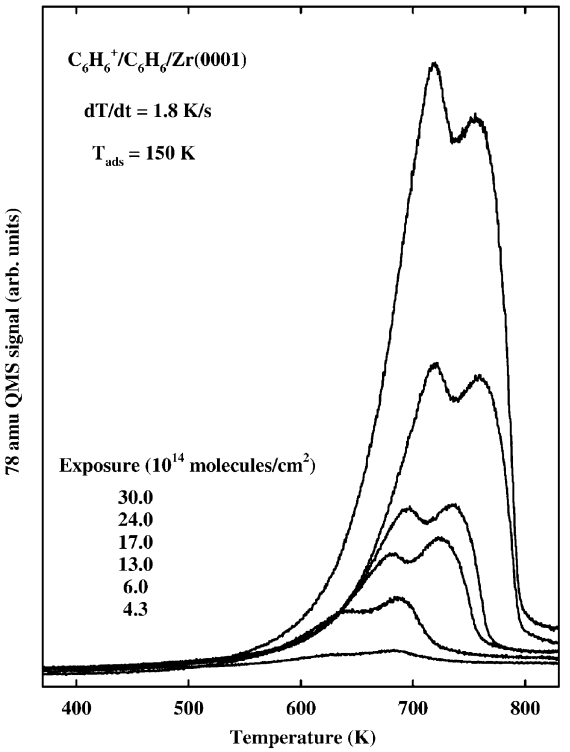

Fig. 2. Benzene TPD spectra following 150 K benzene adsorption on Zr(0001).

have been employed recently in studies of the interaction of C_6H_6 with Zr(0001) using backfilling methods [15,16]. The unexpectedly high desorption temperature observed previously is now confirmed using the beam doser, and we are now able to resolve two desorption states. Note that an exposure of 4.3×10^{14} molecules/cm^2 produces no desorption peak indicating dissociation of C_6H_6 molecules at low exposures. For exposures up to 17.0×10^{14} molecules/cm^2 the higher temperature desorption state has a greater peak height, whereas above 24.0×10^{14} molecules/cm^2 the lower temperature state becomes more dominant. The effect of increased coverage is reflected in a change of the dominant desorption state. Two desorption states may reflect two geometries of adsorbed benzene as was observed on some other metals [4]. These unusually high desorption peak temperatures are indicative of the strong interaction between adsorbed benzene and the

zirconium surface. Desorption peak temperatures of both features shift to higher temperatures with exposure up to 24.0×10^{14} molecules/cm^2 but further exposure up to 30.0×10^{14} molecules/cm^2 leaves the desorption peak temperatures basically unchanged. These observations point to complicated kinetics of C_6H_6 on Zr(0001).

Fig. 3 shows TPD spectra of C_6H_6/Zr(0001) exposed to 500 eV electron bombardment. Desorption peak temperatures of both features shift to higher temperatures with exposure and eventually saturate, similar to what was observed when no electron bombardment was applied. In addition, a fluence of 2×10^{17} electrons/cm^2 resulted in different TPD profiles for exposures below 17.0×10^{14} molecules/cm^2. Note that now the peak height of the lower temperature desorption state dominates for all exposures. Electron bombardment may therefore effect molecular geometry to some extent, favoring the first desorption peak.

Integrated TPD peak areas of benzene as a function of exposure are calculated from spectra in Figs. 2 and 3 and are shown in Fig. 4. Quite unexpectedly, it is difficult to distinguish between these two sets of data. Therefore, we propose that electron bombardment does not affect the amount of desorbing benzene but only the TPD profiles, as Figs. 2 and 3 clearly indicate. Most probably electron impact results in the dissociation of C–H bonds. We propose that hydrogen remains nearby and then recombines and desorbs during heating. This dissociation of C–H bonds induced by electron bombardment could account for the small shift in desorption temperatures. Namely, there are more hydrogen atoms that need to recombine during heating which shifts desorption peaks toward higher temperatures. We have not performed detailed measurements of the electron energy or fluence dependence of these TPD profiles.

It is worth mentioning here that our previous electron-bombardment work involving backfilling (not published) revealed similar trends. Namely,

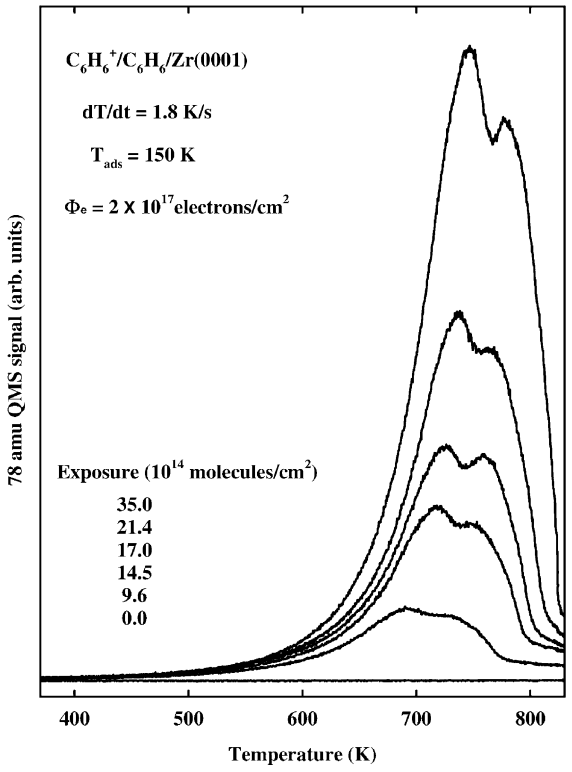

Fig. 3. Benzene TPD spectra following 150 K benzene adsorption on Zr(0001) and 500 eV electron bombardment. The electron fluence is $\Phi_e \sim 2 \times 10^{17}$ electrons/cm^2.

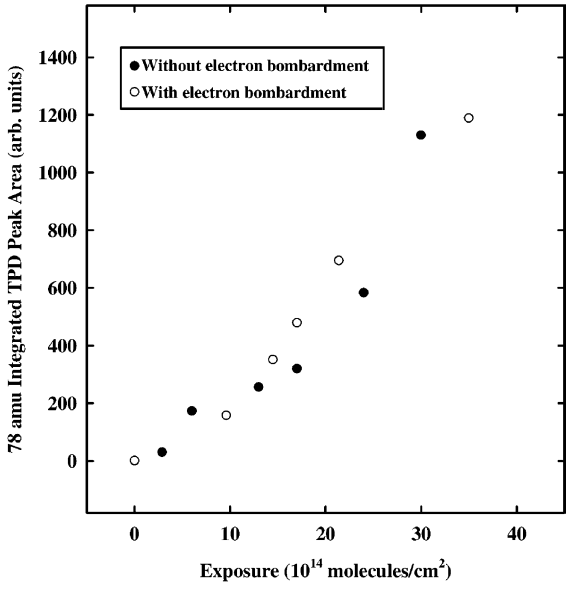

Fig. 4. Benzene integrated TPD area versus benzene exposure. There are no significant effects of electron bombardment on benzene TPD yields.

electron bombardment did not reduce the amount of desorbing benzene as monitored in TPD. However, for backfilling only one desorption peak was observed in TPD, both with and without electron bombardment. These differences are most likely due to desorption from the sample holder assembly in the previous case caused by backfilling the vacuum chamber. Our present results are consistent with our previous work, and provide further insight because of the improved gas-adsorption method.

Fig. 5 shows 78/26 amu ratios versus benzene exposure obtained from integrating TPD areas. These data indicate that there is production of C_2H_2 (26 amu) at lower exposures. With increased exposure, C_6H_6 desorption becomes more prevalent as compared to C_2H_2. Lower 78/26 ratios observed for lower exposures to benzene can be explained by the reactivity of zirconium. Following dissociation of benzene molecules subsequent adsorption proceeds with a lower probability of dissociation. It is unclear at present whether dissociation occurs at 150 K or during TPD experiments. Note that electron bombardment has no effect on this trend.

The dashed line in Fig. 5 indicates the value of the 78/26 amu ratio during dosing, as measured by the QMS positioned out of direct line-of-sight of the molecular beam. Fig. 6, similar to Fig. 5, shows 78/52 amu ratios as a function of exposure. It is evident here that 500 eV electron bombardment also has no detectable effect on the production of C_4H_4. The dashed line indicates the value of 78/52 during dosing. It should be noted that the amount of desorbing benzene (78 amu) compared to all other monitored benzene fragments (77, 51, and 50 amu) have constant values. The fact that electron bombardment does not effect the 78/26 and 78/52 amu ratios is consistent with the fact that electron bombardment does not change the amount of desorbing benzene (Fig. 4). TPD profiles of C_2H_2 and C_4H_4 resemble those of C_6H_6, and our integration procedure includes both peaks.

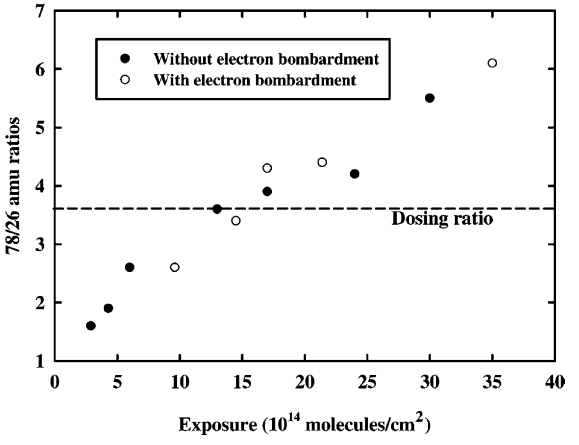

Fig. 5. 78/26 amu ratios obtained from TPD spectra. The dashed line represents this ratio during dosing as detected by the QMS. There are no significant effects of electron bombardment on this ratio.

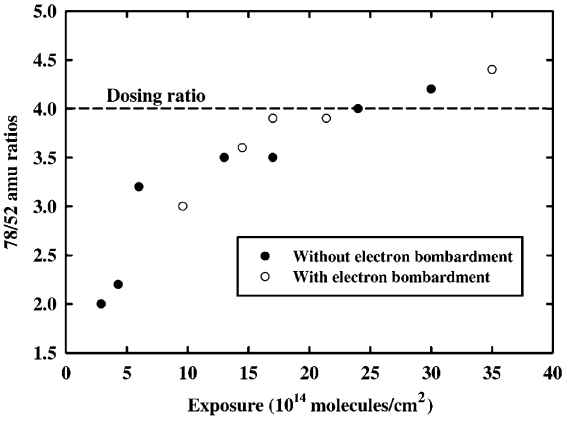

Fig. 6. 78/52 amu ratios obtained from TPD spectra. The dashed line represents this ratio during dosing as detected by the QMS. There are no significant effects of electron bombardment on this ratio.

Electron-induced dissociation of benzene on metal surfaces is a common phenomenon [6,7]. For example, the adsorption of C_6D_6 on Ag(1 1 1) is completely reversible and electron bombardment resulted in decomposition of C_6D_6 to surface D and phenyl fragments [7]. An electron energy slightly above 12 eV was enough to dissociate C–H bonds of benzene on Ag(1 1 1) surface. We propose that like in the case of C_6H_6 on Au(1 1 1) [6], most of the H atoms liberated during electron bombardment stay near the phenyl fragments to recombine and desorb as benzene.

3.2. Auger electron spectroscopy

Fig. 7 presents derivative mode Auger electron spectra for a cleaned Zr(0001) surface and after various benzene exposures. Some carbon and oxygen are always present initially in our experiments. We point out here that keeping the zirconium surface free from carbon, oxygen and sulfur simultaneously is extremely difficult. It is possible, by prolonged annealing at higher temperatures, to dissolve oxygen and carbon into the bulk of this getttering material. However, this would result in sulfur segregation to the surface that we wish to avoid in the present experiments. Several experiments have been conducted with benzene adsorbed on a zirconium surface contaminated with much more carbon and oxygen to determine the role of these impurities. We find that presence of carbon and oxygen on Zr(0001) in greater quantity than we start with after our cleaning cycles has little effect on our TPD data. Namely, the surface is less aggressive toward benzene dissociation since larger 78/26 and 78/52 amu ratios are observed in TPD experiments. However, trends and desorption features resemble those presented here, leading us to conclude that carbon and oxygen contamination does not alter the interpretation of our TPD experiments.

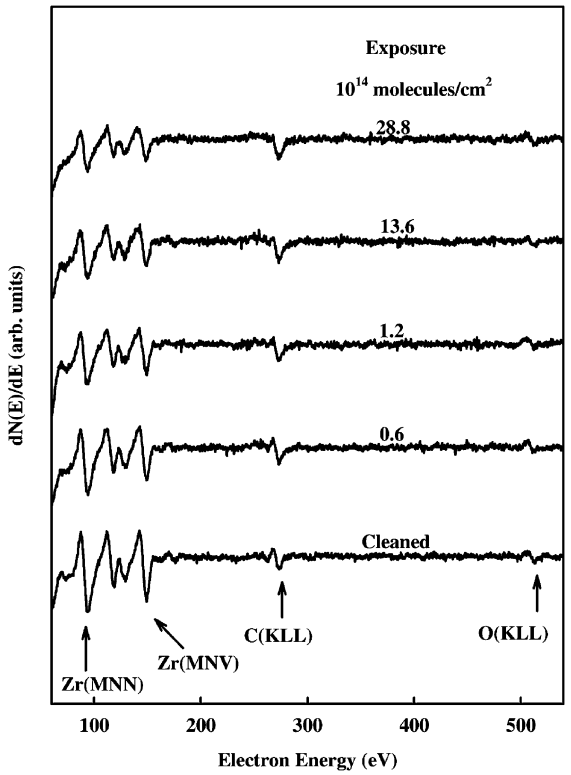

Fig. 7. Auger electron spectra of cleaned and benzene dosed zirconium surfaces. Spectra were taken near 150 K.

In Fig. 7, following exposure of Zr(0001) to benzene, Zr(MNN) and Zr(MNV) Auger features are smaller due to electron attenuation caused by C_6H_6 adsorption. Note that as the exposure is increased, the C(KLL) feature only slightly increases and the presence of carbon is best reflected by the reduction of the zirconium AES features. It should also be stressed that the O(KLL) AES feature is not reduced by benzene adsorption. This was observed previously in our backfilling experiments. The presence of oxygen is possibly induced by the hydrogen from dissociated benzene, which attracts oxygen to the surface from the subsurface region [20]. However, we cannot completely rule out that oxygenic species from the background gas are not adsorbed during benzene dosing.

It is important to note that the carbon C(KLL) feature changes qualitatively following higher exposures to C_6H_6. Based on the feature shape we attribute this to the carbidic form of carbon [2,21] for lower exposures and to a more graphitic form at higher exposures [2]. This is consistent with our TPD results, which indicate that benzene initially dissociates and does not reversibly desorb. The presence of carbon on the surface can be best determined by the C(KLL)/Zr(MNN) Auger peak-to-peak height ratio versus exposure as shown in Fig. 8. For exposures above 10×10^{14} molecules/cm^2 there seems to be saturation behavior, within experimental uncertainty.

Fig. 9 shows how various Auger electron features change upon exposure to benzene and subsequent step-wise annealing. All spectra have been collected at approximately 150 K. Note how the C(KLL) feature becomes larger as the annealing temperature is increased. Annealing up to temperatures where benzene has already desorbed gives the largest carbon AES feature. This is consistent with our discussion that the first adsorbed layer(s)

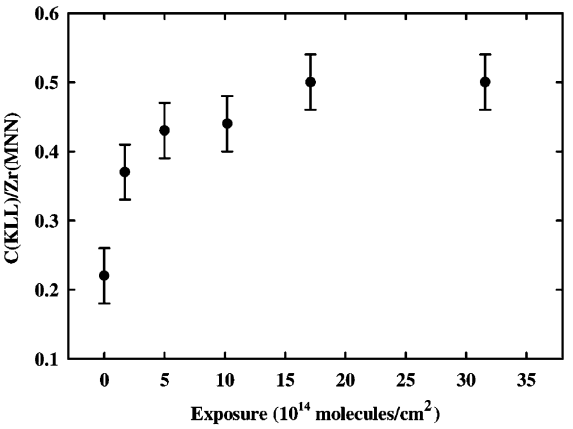

Fig. 8. C(KLL)/Zr(MNN) Auger peak-to-peak height ratios as a function of exposure. Values have been obtained from spectra taken at approximately 150 K.

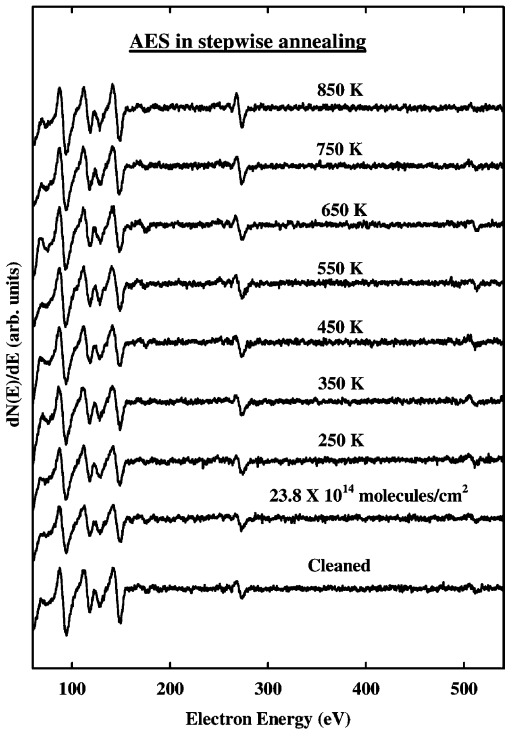

Fig. 9. Auger electron spectra of Zr(0001) after cleaning, exposure to benzene and annealing. Stepwise annealing is performed in 100 K steps from 150 to 850 K and the spectra are collected after cooling to approximately 150 K.

dissociate and with what we observed previously using backfilling. We propose that after desorption the surface is left with more carbon atoms per unit area in the near-surface region making the C(KLL) feature more pronounced. Also note that both the Zr(MNV) and Zr(MNN) features are attenuated following C_6H_6 adsorption. Since no desorption of oxygen-containing molecules is observed in TPD, the reduction of the O(KLL) feature upon annealing to 850 K is due to oxygen diffusion into the bulk. Diffusion of oxygen into the bulk should also contribute to an increase in the C(KLL) feature.

Fig. 10 shows C(KLL)/Zr(MNN) Auger peak-to-peak height ratios an a function of annealing temperature. The values are obtained from the spectra shown in Fig. 9. It is evident that following adsorption of benzene on Zr(0001) the C(KLL)/Zr(MNN) ratio increases and exhibits essentially no changes with annealing up to 650 K. Further annealing to 750 or 850 K increases the C(KLL)/Zr(MNN) ratio. Following benzene desorption one might expect less carbon on the surface, but the zirconium subsurface still retains significant amounts of carbon that migrates to the surface. The presence of different forms of carbon before and after desorption is apparent if one considers the C(KLL) lineshapes in Fig. 9.

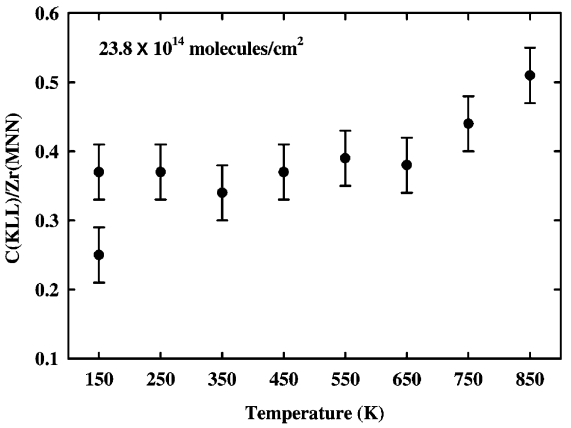

Fig. 10. Auger electron spectra of a stepwise-annealed zirconium surface. Following benzene adsorption at 150 K an increase in the C(KLL)/Zr(MNN) ratio is notable, and a further increase after desorption is evident. The ratios are obtained from the spectra presented in Fig 9.

4. Summary

Following adsorption of C_6H_6 on Zr(0001) at 150 K using a capillary-array molecular beam doser, two desorption states above 700 K are resolved, whereas only one desorption peak was obtained in our recent studies of C_6H_6/Zr(0001) using backfilling [15,16]. We find that the TPD profiles depend both on benzene exposure and electron bombardment. We propose that exposure to electrons effects the geometry of adsorbed molecules, favoring one adsorption state over the other. No effect of electron bombardment on desorption yield is observed in our TPD experiments. We report also on the production of C_2H_2 and C_4H_4 hydrocarbons from benzene at lower exposures. AES C(KLL) features show significant line-shape changes with exposure and annealing. The C(KLL) Auger feature is larger after annealing than immediately after exposure. This indicates that there are more carbon atoms per unit area at the surface after desorption—when only carbidic carbon remains. Oxygen is detected by AES even after C_6H_6 adsorption, and hydrogen from partially dissociated benzene probably plays a role in attracting this oxygen from the subsurface region.

Acknowledgment

Acknowledgement is made to the Donors of the American Chemical Society Petroleum Research Fund for partial support of this research.

References

[1] J.S. Foord, P.J. Goddard, R.M. Lambert, Surf. Sci. 94 (1980) 339.
[2] J.E. Whitten, R. Gomer, Surf. Sci. 347 (1996) 280.
[3] T.-U. Nahm, R. Gomer, Surf. Sci. 356 (1996) 112.
[4] J. Gunster, J. Stultz, S. Krischok, D.W. Goodman, Chem. Phys. Lett. 306 (1999) 335.
[5] M. Xi, M.X. Yang, S.K. Jo, B.E. Bent, P. Stevens, J. Chem. Phys. 101 (1994) 9122.
[6] D. Syomin, J. Kim, B.E. Koel, G.B. Ellison, J. Phys. Chem. B 105 (2001) 8387.
[7] X.-L. Zhou, M.E. Castro, J.M. White, Surf. Sci. 238 (1990) 215.
[8] J. Eng Jr., B.E. Bent, B. Fruhberger, J.G. Chen, J. Phys. Chem. B 101 (1997) 4044.
[9] A.C. Liu, C.M. Friend, J. Chem. Phys. 89 (1998) 4396.
[10] K.M.E. Habermehl-Cwirzen, J. Katainen, J. Lahtinen, P. Hautojarvi, Surf. Sci. 507–510 (2002) 57.
[11] H.H. Graen, M. Neuber, M. Neumann, G. Illing, H.-J. Freund, Surf. Sci. 223 (1989) 33.
[12] P. Jakob, D. Menzel, Surf. Sci. 201 (1988) 503.
[13] W. Braun, G. Held, H.-P. Steinruck, C. Stellwag, D. Menzel, Surf. Sci. 475 (2001) 18.
[14] M. Nishijima, M. Fujisawa, T. Takaoka, T. Sekitani, Surf. Sci. 283 (1993) 121.
[15] N. Stojilovic, R.D. Ramsier, J. Vac. Sci. Technol. A, in press.
[16] N. Stojilovic, R.D. Ramsier, Solid State Commun. 130 (2004) 623.
[17] Y.C. Kang, M.M. Milovancev, D.A. Clauss, M.A. Lange, R.D. Ramsier, J. Nucl. Mater. 281 (2000) 57.
[18] Y.C. Kang, R.D. Ramsier, J. Nucl. Mater. 303 (2002) 125.
[19] N. Stojilovic, J.C. Tokash, R.D. Ramsier, Surf. Sci. 553 (2004) 23.
[20] A. Roustila, J. Chene, C. Severac, J. Alloys Comp. 356–357 (2003) 330.
[21] R.D. Kelley, D.W. Goodman, in: D.A. King, Woodruff (Eds.), The Chemical Physics of Solid Surfaces and Heterogeneous Catalysis, vol. 4, Elsevier, New York, 1982, p. 438.